State the word count for the manuscript: 4116

Usefulness of EBUS-GS and Virtual Bronchoscopic Navigation for Ground-Glass Opacity Lesions

Running head: EBUS-GS and VBN for GGO lesions

Yasuyuki Ikezawa,[a] Naofumi Shinagawa,[a] Noriaki Sukoh,[b] Megumi Morimoto,[a] Hajime Kikuchi,[a] Masahiro Watanabe,[b] Kosuke Nakano,[b] Satoshi Oizumi,[a] and Masaharu Nishimura[a]

[a]First Department of Medicine, Hokkaido University School of Medicine

[b]Respiratory Department, National Hospital Organization Hokkaido Cancer Center

Correspondence and reprint requests to: Naofumi Shinagawa, MD, PhD

First Department of Medicine

Hokkaido University School of Medicine

North 15, West 7, Kita-ku, Sapporo 0608638, Japan

Phone: +81-11-716-1161 (ext. 5911)

Fax: +81-11-706-7899

E-mail: naofu@med.hokudai.ac.jp

Keywords: bronchial endoscopy, ultrasound, EBUS; ultrasound; Lung cancer, diagnosis

State the word count for the abstract: 216

Abstract

Background: Endobronchial ultrasonography with a guide sheath (EBUS-GS) could be useful for diagnosing ground-glass opacity (GGO) predominant-type lesions in the peripheral lung. Furthermore, several studies have reported that transbronchial biopsy (TBB) using EBUS-GS and virtual bronchoscopic navigation (VBN) was safe and effective for diagnosing small peripheral lung lesions. Our objectives were to diagnose solitary peripheral GGO predominant-type lesions by TBB using EBUS-GS and VBN under X-ray fluoroscopic guidance, and to evaluate the clinical factors associated with diagnostic yield.

Methods: The medical records of 169 patients with GGO predominant-type lesions who underwent TBB using EBUS-GS and VBN under X-ray fluoroscopic guidance were retrospectively reviewed.

Results: EBUS images could be obtained for 156 (92%) of 169 GGO predominant-type lesions, and 116 (69%) were successfully diagnosed by this method (20 of 31 pure GGO lesions (65%), 96 of 138 mixed GGO predominant-type lesions (70%)). The mean size of diagnosed lesions was significantly larger than that of nondiagnosed lesions (22 mm vs. 18 mm, $P < 0.01$). Regarding diagnostic yield based on computed tomography sign, cases with presence of a bronchus leading directly to a lesion had significantly higher diagnostic yield

than the other lesions ($P < 0.01$).

Conclusions: The addition of VBN to EBUS-GS could be useful in clinical practice for diagnosing GGO predominant-type lesions in the peripheral lung.

Introduction

Lung cancer is a major health problem worldwide. The majority of patients are diagnosed with advanced and unresectable disease (stage IIIB/IV), which carries a 5-year survival rate of less than 5% [1]. Therefore, it is important to detect and treat lung cancer at an early stage. Recently, due to advances in computed tomography (CT) and increased use of low-dose helical CT in lung cancer screening, small nodules, including solitary peripheral ground-glass opacity (GGO) predominant-type lesions, are being detected with greater frequency [2, 3]. Furthermore, diagnosis of peripheral lung lesions has improved due to the introduction of endobronchial ultrasonography with a guide sheath (EBUS-GS) [4, 5].

GGO is a finding on high-resolution CT (HRCT) that is defined as hazy increased attenuation of the lung with preservation of bronchial and vascular margins. In terms of radiologic characteristics, 2 types of GGO predominant type lesions can be identified: pure GGO is a lesion that has no solid component, while mixed GGO is a lesion that consists of heterogeneous attenuation with a solid component [6-8]. GGO predominant-type lesions on HRCT reflected a lepidic growth pattern of tumor cells microspically, related with presence of EGFR mutation and show slow growth over time [9-10]. Therefore, patients with GGO predominat-type lesions have been reported to have a good prognosis [11-13]. However, several methodologic problems hinder diagnosis of GGO predominant-type lesions by transbronchial biopsy (TBB): (1) the lesions may not be visible under X-ray fluoroscopic

guidance; (2) there is difficulty in identifying accessible bronchial routes to reach peripheral lesions within the time limitation of the procedure; and (3) it is difficult to confirm whether biopsy forceps or a brush can accurately reach the lesions. We previously reported that EBUS-GS could be useful in clinical practice for diagnosing GGO predominant-type lesions in the peripheral lung [14, 15], and recent studies have reported that some of these lesions are likely to be diagnosed as adenocarcinoma or precancerous lesions [14, 16-19].

Virtual bronchoscopic navigation (VBN) is a method in which virtual images of the bronchial path to a peripheral lesion are generated and used as a guide to navigate the bronchoscope [20,21]. Several studies have reported that EBUS-GS with VBN was safe and effective for diagnosing small peripheral lung lesions [22, 23]. Furthermore, another study reported that diagnostic yield for small peripheral lung lesions is significantly increased when VBN is added to EBUS-GS [24].

In the present study, we evaluated the diagnostic yield for GGO predominant-type lesions by TBB using EBUS-GS and VBN, and examined the clinical factors associated with diagnosis of such lesions.

Patients and Methods

Patients

The medical records of 169 patients with GGO predominant-type lesions who underwent TBB

using EBUS-GS and VBN under X-ray fluoroscopic guidance between May 2004 and September 2015 at Hokkaido University Hospital or Hokkaido Cancer Center were retrospectively reviewed. This study was approved by the Institutional Review Board of Hokkaido University Hospital (No. 015-0306), and all patients provided written informed consent for TBB using EBUS-GS. In this study, GGO predominant-type lesions were defined as having a reduction of the maximum tumor area in the mediastinal window (Fig 1B, E) compared with the area in the lung window (Fig 1A, D) on thin-slice CT of ≥50% [25]. Among these lesions, pure GGO was defined as a lesion with no solid component (Fig 1A, B), while mixed GGO was defined as a lesion with heterogeneous attenuation and any solid component (Fig 1D, E). As to whether visible or invisible under X-ray fluoroscopy, we retrospectively confirmed GGO predominant-type lesions in X-ray films before bronchoscopy.

CT signs

CT signs of the lesions were retrospectively reviewed as has been previously reported [26]. The relationship between the lesions and the bronchial or arterial trees was classified into 1 of 5 types according to their radiologic appearance on HRCT as follows: type 1, bronchus (with or without pulmonary artery) leading to the center of the lesion; type 2, bronchus (with or without pulmonary artery) leading to the edge of the lesion; type 3, pulmonary artery alone leading to the center of the lesion; type 4, pulmonary artery alone leading to the edge of the

lesion; and type 5, neither bronchus nor pulmonary artery leading to the lesion. According to these criteria, the medical records of 169 patients who underwent HRCT before TBB were retrospectively reviewed. In order to assess the relationship between the lesions and the bronchial or arterial trees, HRCT images were reviewed by 2 of 3 experienced pulmonologists. When the decision concerning the bronchus-lesion or artery-lesion relationship by 2 of the pulmonologists was not compatible, the third pulmonologist made the final decision.

Virtual bronchoscopic navigation

All patients underwent chest CT to generate VB images to guide bronchoscopy. Based on chest CT data, a VBN system (Bf-Navi; Olympus Ltd, Tokyo, Japan; or DirectPath; Cybernet System Ltd, Tokyo, Japan) was used to detect the bronchial route to the target lesion and to produce the VBN. When the bronchus involved by the lesion was unclear, VB images of the bronchus closest to the lesion were produced.

TBB using EBUS-GS and Virtual bronchoscopic navigation

EBUS was performed using an endoscopic ultrasound system equipped with a 20-MHz mechanical radial-type probe (UM-S20-17R; Olympus Medical Systems, Tokyo, Japan) with an external diameter of 1.4 mm, or with an endoscopic ultrasound system equipped with a 20-MHz mechanical radial-type probe (UM-S20-20S; Olympus) with an external diameter of

1.7 mm. A flexible fiberoptic bronchoscope with a 2.0 mm diameter working channel (BF-P-260F; Olympus) and a guide sheath with an external diameter of 1.9 mm were used for the 1.4-mm probe, and a flexible fiberoptic bronchoscope with a <2.8 mm diameter working channel (BF-1T260; Olympus) and a guide sheath with an external diameter of 2.7 mm were used for the 1.7-mm probe. The bronchoscope was inserted as deeply as possible into the target bronchus under direct vision. An EBUS probe was inserted into the guide sheath, and the probe covered with the guide sheath was then inserted through the bronchoscope working channel and advanced to the GGO predominant-type lesions in order to obtain an EBUS image. EBUS imaging and X-ray fluoroscopy were used to confirm that the probe and guide sheath had reached the lesion. Until the lesions were visualized by EBUS-GS, TBB was assisted by using VBN to guide bronchoscopy. In mixed GGO predominant-type lesions, EBUS images showed one of the following: hyperechoic fine dots (<1 mm in diameter) or hyperechoic linear arcs (primarily around the probe) distributed irregularly within the lesions, or a hypoechoic nodule against the background of a delicate fine change in hypoechoic area with hyperechoic fine dots (Fig 1C). On the other hand, in pure GGO predominant-type lesions, hyperechoic fine dots were slightly seen on EBUS images (Fig 1F). After localizing the lesion using EBUS, the probe was removed to leave the guide sheath in the lesion. Biopsy forceps and a bronchial brush were introduced via the guide sheath, and biopsy and brushing was performed under fluoroscopic guidance for pathologic and cytologic

examination. Biopsy was done six times and brushing three times as a routine.

Diagnosis

We did not use on-site cytology. An experienced pathologist interpreted each histologic and cytologic specimen. Suspicious findings were regarded as negative in our analysis. Final diagnosis was established according to pathologic evidence from biopsy including TBB or surgical procedures.

Statistical analysis

Data were analyzed by using Pearson's χ^2 test. Multivariate analysis was used to identify the factors affecting diagnostic yield. All variables reaching a significance level of 5% in univariate analysis were entered into logistic regression analysis. With regard to lesion size cutoff, we selected 20mm because of sensitivity analysis. Statistical software (Jump Pro 11.0.0; SAS Institute, Japan) was used for all analyses, with significance established at the $P < 0.05$ level.

Results

Diagnostic yield of TBB using EBUS-GS

In all 169 lesions, 31 were pure GGO predominant-type lesions and 138 were mixed GGO predominant-type lesions. Mean diameter of the lesions was 23 (11-53) ± 8 mm. Seventy-four

lesions were in the right upper lobe, 10 were in the right middle lobe, 34 were in the right lower lobe, 39 were in the left upper lobe, and 12 were in the left lower lobe (Table 1). All pure GGO predominant-type lesions and 66 mixed GGO predominant-type lesions were not visible under X-ray fluoroscopy (Table 2, Fig 2). Of the 169 lesions, 116 (69%), including 20 of 31 (65%) pure GGO predominant-type lesions and 96 of 138 (70%) mixed GGO predominant-type lesions, were successfully diagnosed by TBB using EBUS-GS (Table 1, Fig 2). EBUS images could be obtained for 26 of 31 pure GGO predominant-type lesions and 130 of 138 mixed GGO predominant-type lesions. Of these 156 lesions, 111 (71%), including 17 of 26 (65%) pure GGO predominant-type lesions and 94 of 130 (72%) mixed GGO predominant-type lesions, were successfully diagnosed (Fig 2). Two cases of pneumothorax occurred in association with this procedure.

Pathologic diagnosis

The pathologic diagnoses were adenocarcinoma in 114 lesions and inflammation in 2. Ninety-nine lesions diagnosed as adenocarcinoma by TBB using EBUS-GS were resected surgically, 12 were irradiated, and the remaining 3 underwent clinical follow-up. Of 53 lesions undiagnosed by TBB using EBUS-GS, 40 were resected surgically, 10 underwent clinical follow-up, and 3 were irradiated. Especially, of undiagnosed 11 pure GGO predominant-type lesions, 3 lesions are undergoing clinical follow up without size change and two lesions

disappeared. The postoperative final diagnoses were adenocarcinoma in 138 lesions (137 primary, 1 metastasis of the colon) and mucosa-associated lymphoid tissue lymphoma in 1.

Clinical factors associated with diagnostic yield

First, we analyzed the relationships between the characteristics of the lesions and diagnostic yield. When the size of diagnosed lesions was compared with that of nondiagnosed lesions, the former was significantly larger (22 mm vs. 18 mm, respectively; $P < 0.01$) (Table 1). As for diagnostic yield according to lesion size, diagnostic yield was 40% (10 of 25) for lesions <15 mm, 66% (29 of 44) for lesions 15 to 19 mm, and 74% (32 of 43) for lesions 20 to 24 mm, 65% (15 of 23) for lesions 25 to 29 mm and 88% (30 of 34) for lesions >30 mm (Table 3). There was no GGO predominant-type lesion under 10 mm. Next, we analyzed the relationship between diagnostic yield and CT signs on HRCT. Lesions with a type 1 CT sign had significantly higher diagnostic yield than the other types ($P < 0.01$) (Table 2). Finally, we analyzed the relationship between diagnostic yield and visibility of the lesion under X-ray fluoroscopy. When the lesions were confirmed under X-ray fluoroscopy, diagnostic yield was 76%; however, if confirmation was not possible, diagnostic yield decreased to 63% ($P = 0.062$) (Table 2).

Uni- and multivariate analyses of clinical factors affecting diagnostic yield

In univariate analysis, lesion size (>20 mm) and CT sign (type 1) were found to be significant factors predicting diagnostic yield, while lesion visibility under X-ray fluoroscopy showed a tendency to predict diagnostic yield (Table 4). In multivariate analysis, CT sign remained as the only significant factor predicting diagnostic yield ($P < 0.01$) (Table 4).

Comment

Although peripheral GGO predominant-type lesions are difficult to diagnose by bronchoscopy, there have been several reports demonstrating a promising diagnostic yield by TBB using EBUS-GS [14, 27]. This is the first study to demonstrate a promising diagnostic yield for peripheral GGO predominant-type lesions by TBB using EBUS-GS and VBN; of the 169 lesions included in the present study, 116 (69%) were successfully diagnosed by this method. A surprising result was that 20 of 31 pure GGO predominant-type lesions could be successfully diagnosed.

We previously reported that EBUS-GS without VBN could be useful in clinical practice for diagnosing GGO predominant-type lesions in the peripheral lung, and described the advantages of EBUS-GS [14]. Especially, in the case of pure GGO, the change in brightness on EBUS images was very delicate when the EBUS probe was in and out of the lesions (Figure 1c). However, after becoming familiar with the changes of the EBUS images, the positions of pure GGO can be confirmed and EBUS-GS become useful modality to

diagnose pure GGO predominant-type lesions. These advantages are also applicable to TBB using EBUS-GS and VBN. Compared with the results of our previous report, the addition of VBN to EBUS-GS increased the arrival rate to GGO predominant-type lesions (50/67 [75%] vs. 156/169 [92%]) as well as diagnostic yield (38/67 [57%] vs. 116/169 [69%]). Moreover, in pure GGO predominant-type lesions, the addition of VBN to EBUS-GS increased the arrival rate (6/11 [55%] vs. 26/31 [84%]) and diagnostic yield (5/11 [45%] vs. 20/31 [65%]). These results show that the addition of VBN to EBUS-GS could be more useful than EBUS-GS alone for obtaining EBUS images and diagnosing GGO predominant-type lesions.

In this study, we examined the relationships between the characteristics of the lesions and diagnostic yield by using uni- and multivariate analyses. In these analyses, CT sign was the most important factor. However, of 41 lesions with a CT sign of type 3 to 5 (type3, pulmonary artery alone leading to the center of the lesion; type4, pulmonary artery alone leading to the edge of the lesion; type5, neither bronchus nor pulmonary artery leading to the lesion), 37 (90%) were confirmed on EBUS-GS and 22 (54%) were successfully diagnosed. Furthermore, of 61 diagnosed lesions that were not visible under X-ray fluoroscopy, 57 were considered to be “within image” or “adjacent to image” on EBUS. These results indicate that producing VBN to the bronchus that was central or closest to the lesion contributed to successfully reaching the lesion, obtaining EBUS-GS images of the lesion, and increasing diagnostic yield.

Lee et al reported that when pure GGO predominant-type lesions are greater than 15 mm in diameter with nodularity or harbor a solid component within them, the lesions are more likely to be invasive adenocarcinoma [28]. Furthermore, in this study, the rate of diagnosed malignancy was high and the diagnostic yield of lesions under 15mm was low (Table3). These suggest that we should not bronchospically approach all GGO predominant-type lesions. The patients who are low risk for an operation had better go directly to surgical resection if they are suspicious, <15mm pure GGO or mixed GGO predominant-type lesions and we should select and bronchospically approach GGO predominant-type lesions of the patients who were high risk for an operation when (1) pure GGO predominant-type lesions are greater than 15 mm in diameter or (2) solid components newly emerge and are getting greater or (3) GGO predominant-type lesions have solid components because of its invasion.

There are some major limitations in the present study. The first is the retrospective nature of the study. As such, there might have been some selection bias for the examined cases, and inspection duration was not recorded. Furthermore, no control group was set for comparison. The second is that the technique of the physicians might have affected diagnostic yield. However, in order to minimize variability, all bronchoscopies were performed by well-trained bronchoscopists. The third was that we could not show the pathological results in accordance with new ATS/IASLC/ERS classification for surgical specimens before

2011 because the pathological surgical specimens were diagnosed between May 2004 and September 2015.

In conclusion, the addition of VBN to EBUS-GS could be useful in clinical practice for diagnosing GGO predominant-type lesions in the peripheral lung. However, further prospective randomized studies are necessary to clarify its usefulness.

Financial Disclosure and Conflicts of Interest

All authors have no conflicts of interest to declare.

References

1. Yang P, Allen MS, Aubry MC, et al. Clinical features of 5,628 primary lung cancer patients: experience at Mayo Clinic from 1997 to 2003. Chest 2005; 128: 452-462

2. Henschke CI, Yankelevitz DF, Mirtcheva R, et al. CT screening for lung cancer: frequency and significance of part-solid and nonsolid nodules. AJR Am J Roentgenol 2002; 178: 1053-1057

3. Li F, Sone S, Abe H, MacMahon H, Doi K. Malignant versus benign nodules at CT screening for lung cancer: comparison of thin-section CT findings. Radiology 2004; 233: 793-798

4. Huang CT, Tsai YJ, Liao WY, et al. Endobronchial ultrasound-guided transbronchial biopsy of peripheral pulmonary lesions: how many specimens are necessary? Respiration 2012; 84: 128-134

5. Gompelmann D, Herth FJ. Role of endobronchial and endoscopic ultrasound in pulmonary medicine. Respiration 2014; 87: 3-8

6. Nakajima R, Yokose T, Kakinuma R, Nagai K, Nishiwaki Y, Ochiai A. Localized pure ground-glass opacity on high-resolution CT: histologic characteristics. J Comput Assist Tomogr 2002; 26: 323-329

7. Austin JH, Muller NL, Friedman PJ, et al. Glossary of terms for CT of the lungs: recommendations of the Nomenclature Committee of the Fleischner Society. Radiology 1996;

200: 327-331

8. Nakata M, Saeki H, Takata I, et al. Focal ground-glass opacity detected by low-dose helical CT. Chest 2002; 121: 1464-1467

9. Kuriyama K, Seto M, Kasugai T, et al. Ground-glass opacity on thin-section CT: value in differentiating subtypes of adenocarcinoma of the lung. Am J Roentgenol 1999;173: 465-469.

10. Yano M, Sasaki H, Kobayashi Y, et al. Epidermal growth factor receptor gene mutation and computed tomographic findings in peripheral pulmonary adenocarcinoma. J Thorac Oncol 2006; 1: 413-416.

11. Kim EA, Johkoh T, Lee KS, et al. Quantification of ground-glass opacity on high resolution CT of small peripheral adenocarcinoma of the lung: pathologic and prognostic implications. AJR Am J Roentgenol 2001; 177:1417-1422.

12. Kodama K, Higashiyama M, Yokouchi H, et al. Prognostic of ground-glass opacity found in small lung adenocarcinoma on high resolution CT scanning. Lung Cancer 2001; 33:17-25.

13. Asamura H, Hishida T, Suzuki K, et al. Radiographically determined noninvasive adenocarcinoma of the lung: survival outcomes of Japan Clinical Oncology Group 0201. J Thorac CardiovascSurg 2013; 146:24-30.

14. Ikezawa Y, Sukoh N, Shinagawa N, Nakano K, Oizumi, Nishimura M. Endobronchial ultrasonography with a guide sheath for pure or mixed ground-glass opacity lesions. Respiration 2014; 88: 137-143.

15. Sukoh N, Shinagawa N, Ikezawa Y, et al. Characteristics of endobronchial ultrasonographic (EBUS) images in three cases with ground glass opacity (GGO) predominant-type peripheral pulmonary lesions (PPLs). J Jpn Soc Bronchology 2014; 36: 298-303

16. Matsunaga H, Yokoi K, Anraku M, et al. Proportion of ground-glass opacity on high-resolution computed tomography in clinical T1 N0 M0 adenocarcinoma of the lung: a predictor of lymph node metastasis. J Thorac Cardiovasc Surg 2002; 124: 278-284

17. Park CM, Goo JM, Lee HJ, Lee CH, Chun EJ, Im JG. Nodular ground-glass opacity at thin-section CT: histologic correlation and evaluation of change at follow-up. Radiographics 2007; 27: 391-408

18. Lee HJ, Goo JM, Lee CH, Yoo CG, Kim YT, Im JG. Nodular ground-glass opacities on thin-section CT: size change during follow-up and pathological results. Korean J Radiol 2007; 8: 22-31

19. Kim HY, Shim YM, Lee KS, Han J, Yi CA, Kim YK. Persistent pulmonary nodular ground-glass opacity at thin section CT: histopathologic comparison. Radiology 2007; 245: 267-275

20. Asano F, Kimura T, Shindou J, et al. Usefulness of CT-guided ultrathin bronchoscopy in the diagnosis of peripheral pulmonary lesions that could not be diagnosed by standard transbronchial biopsy. J Jpn Soc Bronchology 2002; 24: 80-85

21. Shinagawa N, Yamazaki K, Onodera Y, et al. CT-guided transbronchial biopsy using an ultrathin bronchoscope with virtual bronchoscopic navigation. Chest 2004; 125: 1138-1143

22. Asahina H, Yamazaki K, Onodera Y, et al. Transbronchial biopsy using endobronchial ultrasonography with a guide sheath and virtual bronchoscopic navigation. Chest 2005; 128: 1761-1765

23. Asano F, Matsuno Y, Shinagawa N, et al. A virtual bronchoscopic navigation system for pulmonary peripheral lesions. Chest 2006; 130: 559-566

24. Ishida T, Asano F, Yamazaki K, et al. Virtual bronchoscopic navigation combined with endobronchial ultrasound to diagnose small peripheral lesions: a randomised trial. Thorax 2011; 66: 1072-1077

25. Suzuki R, Yamada K, Noda K. Atypical adenomatous hyperplasia of the lung: correlation between thin-section computed tomography findings and histopathologic features. Jpn J Lung Cancer 2003; 43: 105-112

26. Shinagawa N, Yamazaki K, Onodera Y, et al. Factors related to diagnostic sensitivity using an ultrathin bronchoscope under CT guidance. Chest 2007; 131: 549-553

27. Izumo T, Sasada S, Chavez C, Matsumoto Y, Tsuchida T. Radial endobronchial ultrasound images for ground-glass opacity pulmonary lesions. Eur Respir J 2014; 45: 1661-1668

28. Lee HY, Choi YL, Lee KS et al. Pure ground-glass opacity neoplastic lung nodules: Histopathology, imaging, and management. AJR 2014; 202:224-233.

Table 1. Characteristics of diagnosed and nondiagnosed lesions

Characteristic	Diagnosed (n = 116)	Nondiagnosed (n = 53)	P value
Age, median (range), y	71 (39–85)	70 (39–82)	0.67
Sex, M/F, n	39/77	22/31	0.33
Location of lesion, n			0.23*
Right upper lobe	53	21	
Right middle lobe	6	4	
Right lower lobe	23	11	
Left upper lobe	25	14	
Left lower lobe	9	3	
Lesion size, median ± SD, mm	22.0 ± 8.9	18.0 ± 6.4	<0.01
Pure/mixed GGO, n	20/96	11/42	0.71

*Right upper lobe vs. others.

Abbreviation: GGO, ground-glass opacity.

Table 2. Clinical factors associated with diagnostic yield of TBB using EBUS-GS

Variable	Diagnosed by EBUS-GS/total lesions, n (%)	P value
CT sign		<0.01*
Type 1	78/99 (79)	
Type 2	16/29 (55)	
Type 3	16/25 (64)	
Type 4	5/13 (38)	
Type 5	1/3 (33)	
X-ray fluoroscopy		0.062
Visible	55/72 (76)	
Invisible	61/97 (63)	

*Type 1 vs. others.

Abbreviations: CT, computed tomography; EBUS-GS, endobronchial ultrasonography with a guide sheath; TBB, transbronchial biopsy.

Table 3. Diagnostic yield of EBUS-GS

Lesion size, mm	Total, n (%)	Pure GGO, n (%)	Mixed GGO, n (%)
<15	10/25 (40)	4/6 (67)	6/19 (32)
15–19	29/44 (66)	8/13 (61)	21/31 (68)
20-24	32/43 (74)	5/8 (63)	27/35 (77)
25-29	15/23 (65)	1/2 (50)	14/21 (67)
30<	30/34 (88)	2/2 (100)	28/32 (88)
Total	116/169 (69)	20/31 (65)	96/138 (70)

Abbreviations: EBUS-GS, endobronchial ultrasonography with a guide sheath; GGO, ground-glass opacity.

Table 4. Logistic regression analysis of clinical factors affecting diagnostic yield

	Univariate		Multivariate	
Variable	HR (95% CI)	P Value	HR (95% CI)	P Value
Lesion size (>20 vs. ≤20 mm)	2.6 (1.3–5.1)	<0.01	1.9 (0.8–3.7)	0.13
CT sign 1 vs. others	3.1 (1.6–6.2)	<0.01	2.8 (1.1–4.9)	0.02
Visible vs. invisible	1.9 (1.0–3.8)	0.059	1.4 (0.7–2.9)	0.37
Pure vs. mixed GGO	1.3 (0.5–2.8)	0.59		

Abbreviations: CI, confidence interval; HR, hazard ratio; GGO, ground-glass opacity.

Figure Legends

Fig 1.

A. Thin-section computed tomographic (CT) image, showing homogeneous focal translucent pure ground-glass opacity (GGO) in the lung window.

B. Thin-section CT image, showing no solid component in the mediastinum.

C. Endobronchial ultrasound (EBUS) image, showing pure GGO with a delicate high-echoic pattern compared with normal lung tissue.

D. Thin-section CT image, showing homogeneous focal translucent mixed GGO with solid components in the lung window.

E. Thin-section CT image, showing some solid components in the mediastinum.

F. EBUS image, showing mixed GGO characterized by a low-echoic nodule surrounded by a highly reflective interface between the aerated lung and the lesion.

Fig 2. Flow diagram of 169 ground-glass opacity predominant-type lesions.

figure1

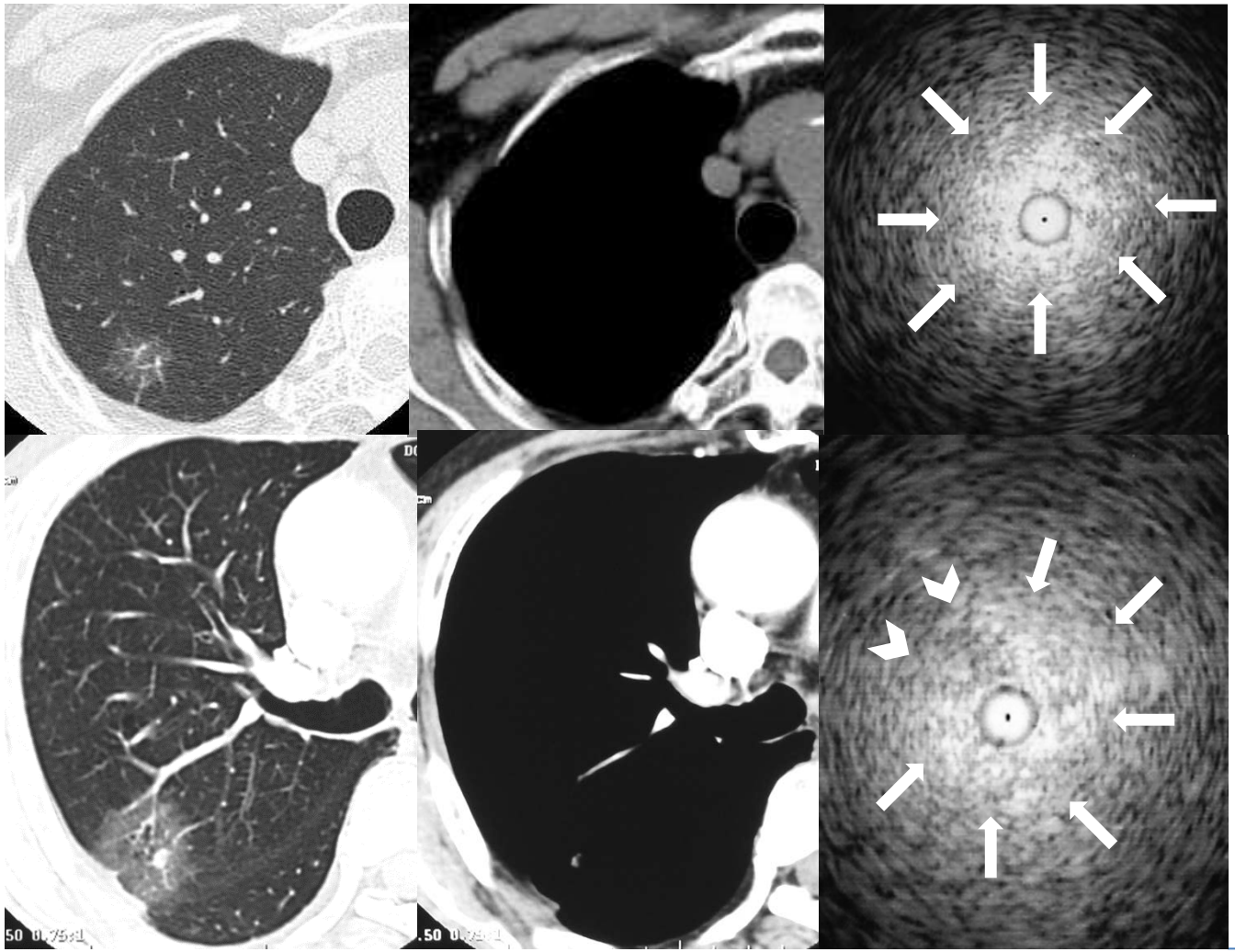

a	b	c
d	e	f

figure 2

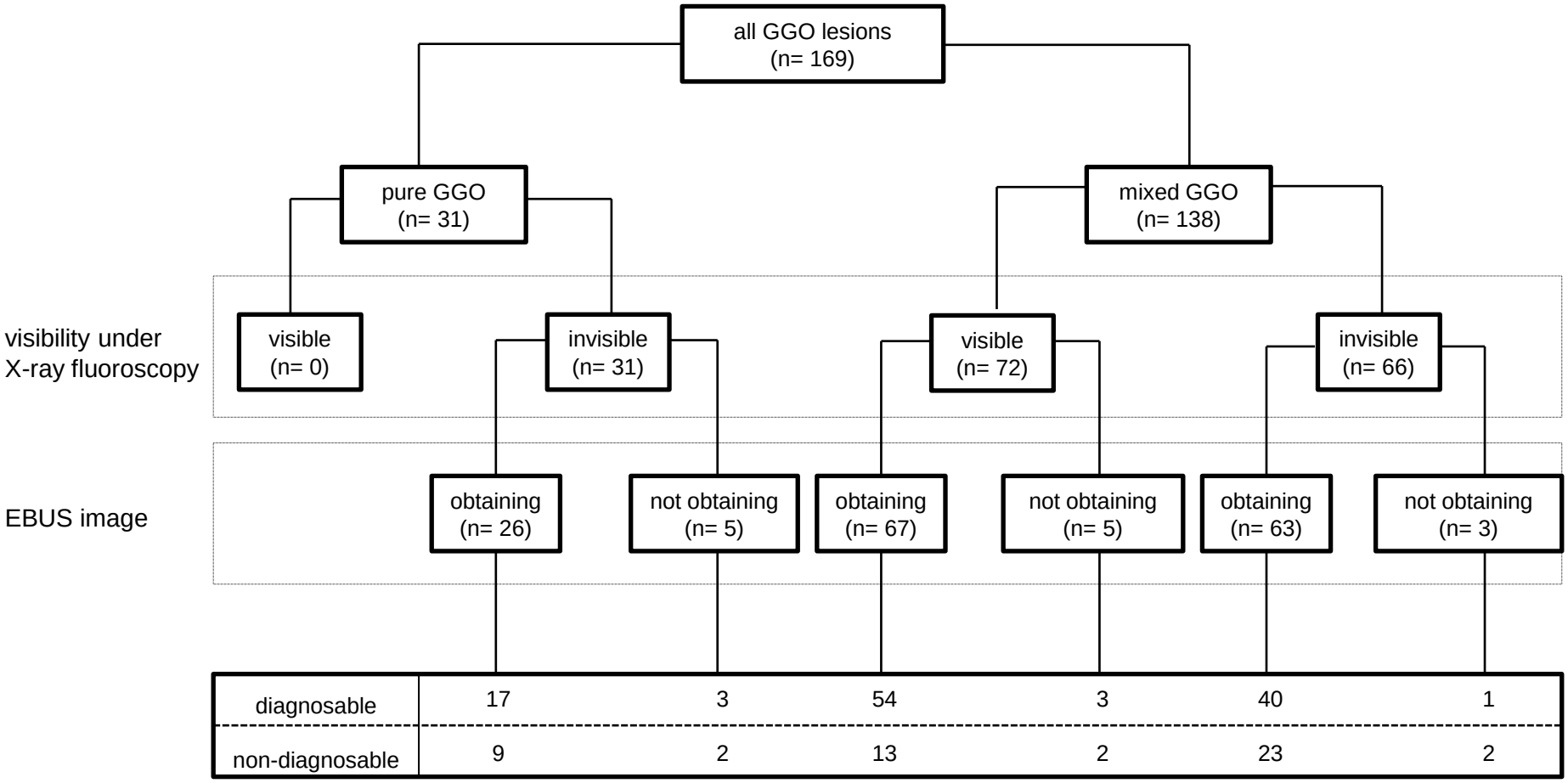
all GGO lesions
(n= 169)
pure GGO
(n= 31)
mixed GGO
(n= 138)
visibility under
X-ray fluoroscopy
visible
(n= 0)
invisible
(n= 31)
visible
(n= 72)
invisible
(n= 66)
EBUS image
obtaining
(n= 26)
not obtaining
(n= 5)
obtaining
(n= 67)
not obtaining
(n= 5)
obtaining
(n= 63)
not obtaining
(n= 3)
diagnosable
17
3
54
3
40
1
non-diagnosable
9
2
13
2
23
2